Effect of interaction between ion drag and conduction on electrohydrodynamic pumping

Masahito Nishikawara, Kota Shomura, Hideki Yanada

nishikawara@me.tut.ac.jp

Abstract

Electrohydrodynamics (EHD) flow is induced by Coulomb force acting on excess charges in a dielectric fluid under a high electric field and can be applied to pumping. There are two types of EHD pump, ion drag pump and conduction pump that utilize excess charges caused by charge injection and electric field enhanced dissociation, respectively. This paper investigates numerically the interaction of the ion drag action and conduction action on EHD pump characteristics using three types of electrode configurations. It is found that when the ion drag and conduction act simultaneously, the developed pressure is augmented and is higher than the sum of the pressures developed separately by each action, and that the degree of pressure augmentation strongly depends on electrode configuration.

1 INTRODUCTION

Electrohydrodynamics (EHD) flow is induced by CoulombвЃ™s force acting on excess charges in a dielectric fluid under a high electric field and can be applied to pumping and heat transfer. Excess charges in the fluid are generated by charge injection from an electrode and/or a non-equilibrium state of dissociation-recombination of dissociative molecules. An EHD pump that utilizes the former phenomenon is called the ion drag pump and the one that utilizes the latter phenomenon is called the conduction pump. Both types of EHD pump have been widely investigated experimentally and numerically[1, 2, 3, 4]. However, the research on the interaction of the two charge generation phenomena is very limited[3]. This paper investigates numerically the effect of the interaction of the two charge generation phenomena on EHD pump characteristics.

2 NUMERICAL MODELING

The governing equations are the continuity equation (Eq. (1)), the NaviervYS-tokesвЃ™ equation (Eq.(2)) including Coulomb's force (Eq. (3)) as an external force, GaussвЃ™ law (Eq. (4)) and the charge conservation equations (Eqs. (6)-(10)).

$$\nabla \cdot \mathbf{v} = \mathbf{0} \tag{1}$$

$$(\mathbf{v} \cdot \nabla)\mathbf{v} = -\frac{\mathbf{1}}{\mathbf{æ}}\nabla \mathbf{p} + \mathbf{v}\nabla^{\mathbf{2}}\mathbf{v} + \mathbf{f} \tag{2}$$

$$\mathbf{f} = -\frac{\mathbf{q_{total}}}{\mathbf{æ}}\nabla \mathbf{Œ} \tag{3}$$

$$\nabla^2 \phi = -\frac{q_{total}}{\varepsilon} \tag{4}$$

$$q_{total} = q_{in} + q - w \tag{5}$$

In the equations, $\mathbf{v}$=(u, v) is the velocity,ρ is the density, p is the pressure, v is the kinematic viscosity, $\mathbf{f}$ is the Coulomb's force, q_{total} is the total charge density defined by Eq. (5), ϕ is the electric potential, ε is the permittivity, q_{in} is the positive charge density injected from a positive electrode, q and w are the densities of the positive and negative charges generated by dissociation, respectively. In this model, it is assumed that only positive charges are injected and that the injected positive charges are not combined with the negative charges generated by the dissociation. The charge conservation equations of the injected charges and dissociated ones are described separately as follows[2].

$$\nabla \cdot \mathbf{j}_{\mathrm{in}} = \mathbf{0} \tag{6}$$

$$\mathbf{j}_{\mathrm{in}} = {}^{-}{}_{\mathbf{in}}\mathbf{q}_{\mathbf{in}}\mathbf{E} + \mathbf{q}_{\mathbf{i}}\mathbf{n}\mathbf{v} - \mathbf{D}_{\mathbf{i}}\nabla \mathbf{q}_{\mathbf{i}}\mathbf{n} \tag{7}$$

$$\nabla \cdot \mathbf{j} = \mathbf{k}_{\mathbf{r}}\left(\mathbf{w}_{\mathbf{0}}^{\mathbf{2}}\mathbf{F}(\mathbf{E}) - \mathbf{q}\mathbf{w}\right) \tag{8}$$

$$\mathbf{j}_{+} = {}^{-}{}_{\mathbf{i}} + \mathbf{q}\mathbf{E} + \mathbf{q}\mathbf{v} - \mathbf{D}_{\mathbf{i}}\nabla \mathbf{q} \tag{9}$$

$$\mathbf{j}_{-} = {}^{-}{}_{\mathbf{i}} - \mathbf{w}\mathbf{E} + \mathbf{w}\mathbf{v} - \mathbf{D}_{\mathbf{i}}\nabla \mathbf{w} \tag{10}$$

j_{in} is the current density of the injected charge, μ_{in} is its mobility, E is the electric field strength, D_i is the charge diffusion constant, j_+ and j_- are the current densities of the dissociated positive and negative charges, respectively, k_r is the recombination rate constant, w_0 is the negative charge density at an equilibrium (=q_0), F(E) is a function representing the field enhanced dissociation, $\mathrm{Oë}_{i+}$ and $\mathrm{Oë}_{i-}$ are the mobilities of the positive and negative dissociated charges, respectively. It is assumed for simplicity that $\mathrm{Oë}_{in}$=$\mathrm{Oë}_{i+}$=$\mathrm{Oë}_{i-}$. To obtain F(E), an electric field dependence of the electric conductivity of dibutyl sebacate (DBS) was measured in laboratory using concentric cylinder electrodes [5]. Linear approximation was used to determine F(E).

$$F(E) = \frac{k_d}{k_{d0}} = \left(\frac{\sigma}{\sigma_0}\right)^2 \tag{11}$$

$$\frac{\sigma}{\sigma_0} = \gamma E + 1 \tag{12}$$

k_d is the dissociation constant, σ is the electric conductivity. The results is shown in Fig.1. It was found from the measurement that $\gamma = 2.46$ГЧ10^{-7} m/V for DBS. The field dependence of the electric conductivity was calculated from Onsager theory[6] and it was found that $\gamma =1.31$ГЧ10^{-7} m/V. The measurement result was larger than the value predicted from the theory. In this numerical simulation, the measured value was used.
The recombination rate constant k_r and the negative charge density at equilibrium, w_0 are expressed by

$$k_r = \frac{\mu_+ + \mu_-}{\varepsilon} \tag{13}$$

$$w_0 = \frac{\sigma_0}{\mu_+ + \mu_-} \tag{14}$$

The charge density, q_e, injected from an electrode can be given by Eq. (15)[4],

$$q_e = k(E_{static} - E_{thres}) \tag{15}$$

where k is the proportionality constant, E_{static} is a mean value of the electrostatic field strength at the charge injection region (see Fig. 2) and E_{thres} is the threshold value of E_{static} below which no charge injection takes place. The model detail is presented in Refs. [1, 2, 3].

3 ELECTRODE CONFIGURATION

Three EHD pumps with different electrode configurations in Fig. 2 are simulated. Plate-bar electrodes, two-plate electrodes mounted on the wall, and embedded two-plate electrodes are inserted in a two-dimensional flow channel. The geometries of the three types of electrodes are symmetrical about the centerline and, therefore, numerical simulations were conducted using half models in Fig. 1. The dimensions of the computational domain are 0.5 mm height and 8 mm length. The plate-bar electrodes consist of a plate 0.1 mm thickness and 0.5 mm length located in the center of the flow channel, and of two square bars with a cross-section of 0.3 ГЧ 0.3 mm2 mounted on the walls. The plate electrode is connected to a positive high voltage (HV) and the square bar electrodes are grounded. The two-plate electrodes on the wall consist of plate electrodes with different lengths of 0.15 mm and 0.5 mm and their thickness is 0.1 mm. The short electrode is connected to the positive high voltage and the long one is grounded. The two-plate electrodes embedded in the wall are basically the same as the two-plates electrodes mounted on the wall, except that the electrode surface is flush with the channel wall. The gap between the electrodes is 0.2 mm for the three types of electrodes. Numerical simulations were made for three cases: (1) only charge injection phenomenon (ion drag action), (2) only non-equilibrium phenomenon of dissociation-recombination (conduction action), and (3) both phenomena (ion drag + conduction actions) take place. Inlet flow rate is imposed as a boundary condition from zero to a maximum, at which the pressure

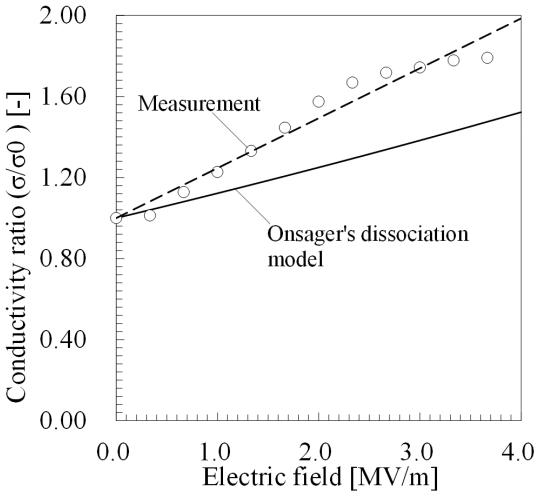

Figure 1: Electric field dependence of conductivity.

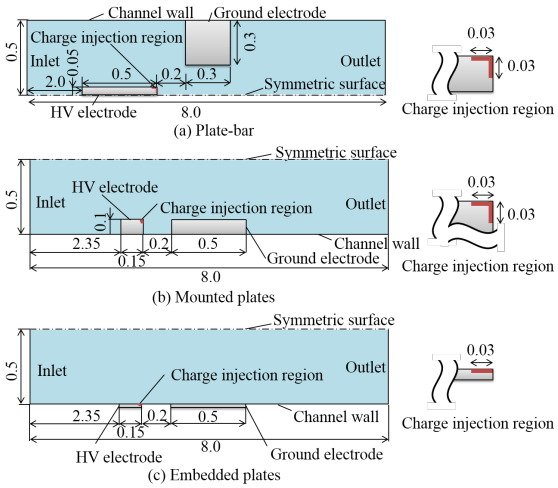

Figure 2: Electrode configuration (not to scale) (unit : mm).

difference between the outlet and inlet of the computational domain is zero, to obtain the pressure-flowrate characteristics. Charge injection region is imposed at a corner of each high voltage electrode, as shown in Fig. 2.
Table 1 Working fluid properties.

Table 15: Working fluid properties.

Fluid	Dibutyl sebacate (DBS)
Density [kg/m^3][7]	938
Relative permittivity [-]	4.5
Conductivity[S/m]	3.41×10^{-10}
Viscosity [Pa·s]	7.50×10^{-3}
Ionic mobility [m/V·s]	2.77×10^{-9}
k in Eq. (10) [C/V·m^3]	7.03×10^{-9}
E_{thres} in Eq. (10) [V/m]	0.245×10^{6}

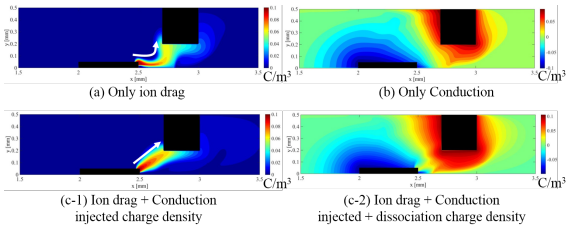

Figure 3: Charge density distribution (Ve=1.2 kV , Uin=0 m/s). Note that range of color bar of (a, c-1) and (b, c-2) is different.

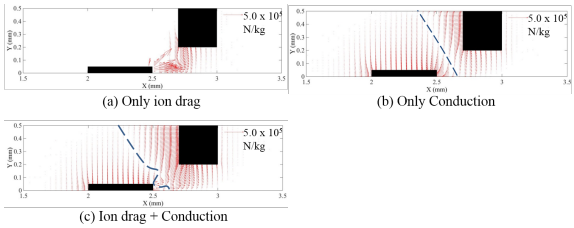

Figure 4: Coulomb's force distribution (Ve=1.2 kV , Uin=0 m/s). Dashed line is the boundary where the force is zero.

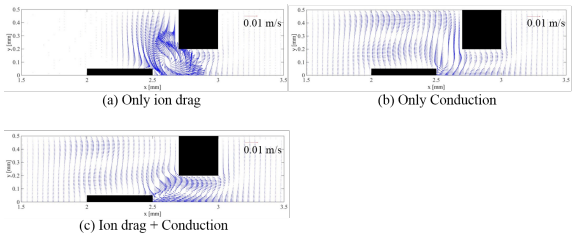

Figure 5: Flow velocity distribution (Ve=1.2 kV , Uin=0 m/s).

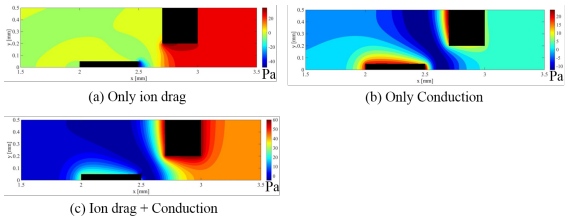

Figure 6: Pressure distribution (Ve=1.2 kV , Uin=0 m/s). Note that range of color bar is different.

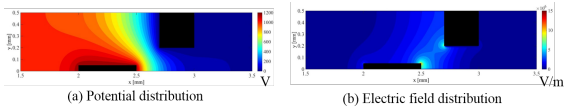

Figure 7: Distribution of potential and electric field (Ve=1.2 kV , Uin=0 m/s). Results of both ion drag and conduction actions.

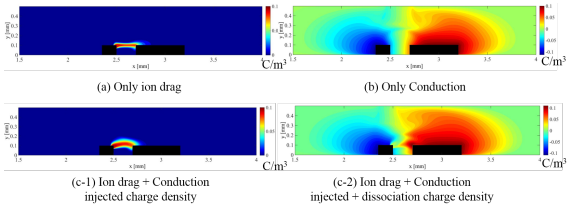

Figure 8: Charge density distribution (Ve=2.0 kV , Uin=0 m/s). Note that range of color bar of (a, c-1) and (b, c-2) is different.

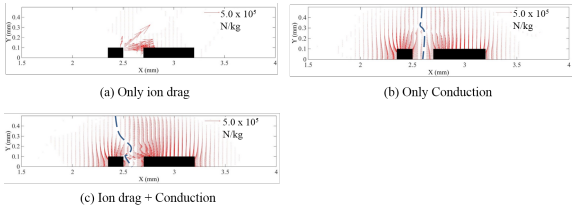

Figure 9: Coulomb's force distribution (Ve=2.0 kV , Uin=0 m/s). Dashed line is the boundary where the force is zero.

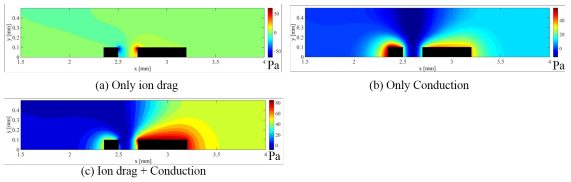

Figure 10: Pressure distribution (Ve=2.0 kV , Uin=0 m/s). Note that range of color bar is different.

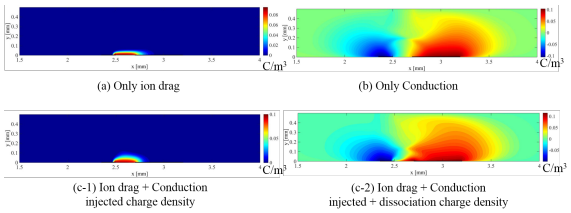

Figure 11: Charge density distribution (Ve=2.0 kV , Uin=0 m/s). Note that range of color bar of (a, c-1) and (b, c-2) is different.

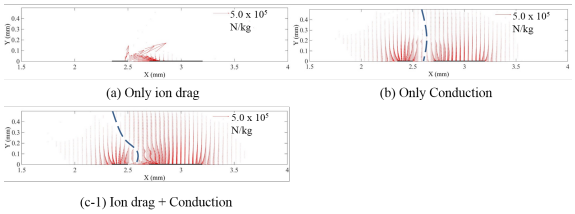

Figure 12: Coulomb's force distribution (Ve=2.0 kV , Uin=0 m/s). Dashed line is the boundary where the force is zero.

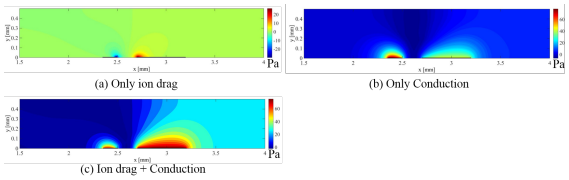

Figure 13: Pressure distribution (Ve=2.0 kV , Uin=0 m/s). Note that range of color bar is different.

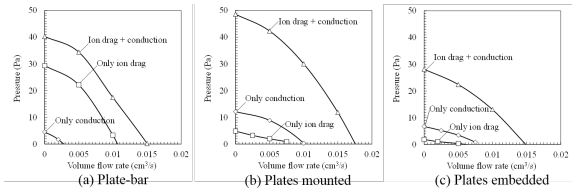

Figure 14: Pressure - flow rate characteristics (Ve=1.2 kV for (a) and 2.0 kV for (b) and (c)).The flow rate is calculated as the channel depth of 5mm.

In the simulation, physical properties of dibutyl sebacate (DBS, C18H34O4) as working fluid were used and are listed in Table 1. A cone-plate rotational viscometer (TOKI SANGYO RE80) was used for viscosity measurement. Relative permittivity was measured using a probe consisting of two concentric cylinders (RUFUTO Model 871). The proportionality constant k in Eq. (15) was determined by fitting the simulated pump pressure to the measured pressure when the flow rate is zero4. The ionic mobility was determined by the Walden's rule. Boundary conditions are listed in Table 2, where n stands for the unit normal vector.
Table 2 Boundary conditions.

Table 16: Boundary conditions.

Boundary location	Boundary conditions						Equation number
1. Inlet	$u = U_{in}(y)$	$v = 0$	$q = 0$	$w = 0$	$q_{in} = 0$	$\frac{\partial \phi}{\partial x} = 0$	(16)
2. Outlet	$\frac{\partial u}{\partial x} = 0$	$\frac{\partial v}{\partial x} = 0$	$\frac{\partial q}{\partial x} = 0$	$\frac{\partial w}{\partial x} = 0$	$\frac{\partial q_{in}}{\partial x} = 0$	$\frac{\partial \phi}{\partial x} = 0$	(17)
3. Channel wall	$u = 0$	$v = 0$				$\frac{\partial \phi}{\partial y} = 0$	(18)
4. Symmetrical surface	$\frac{\partial u}{\partial y} = 0$	$v = 0$	$\frac{\partial q}{\partial y} = 0$	$\frac{\partial w}{\partial y} = 0$	$\frac{\partial q_{in}}{\partial y} = 0$	$\frac{\partial \phi}{\partial y} = 0$	(19)
5. Surface of ground electrode	$u = 0$	$v = 0$	$\mathbf{n} \cdot \nabla q = 0$	$w = 0$		$\phi = 0$	(20)
6. Charge injection region	$u = 0$	$v = 0$	$q = 0$	$\mathbf{n} \cdot \nabla w = 0$	$q_{in} = q_e$	$\phi = V_e$	(21)
6'. Surface of HV electrode except for 6	$u = 0$	$v = 0$	$q = 0$	$\mathbf{n} \cdot \nabla w = 0$	$q_{in} = 0$	$\phi = V_e$	(22)

4 RESULTS AND DISCUSSION

Plate-bar electrodes

The distributions of charge density, Coulomb's force, flow velocity, pressure, potential and electric field are shown in Figs. 3-7. The cases for ion drag action,

conduction action, and ion drag and conduction actions are compared at the applied voltage of +1.2 kV and zero net flow rate.

Figure 3(a) shows the injected charge density distribution under no dissociation (no conduction action). For this case, the injected charges do not spread in y direction. Dissociation charges are generated more in higher electrode areas and surround the electrode with a sign opposite to the charges as shown in Fig. 3(b). When both charge injection (ion drag action) and dissociation (conduction action) take place, as can be seen by comparing Fig. 3(a) to Fig. 3(c-2), the injected charge density distribution changes to a straighter and thicker distribution from the HV electrode to the ground electrode. This change is caused by the conduction flow attracting to the HV electrode as shown in Fig. 5(b).

The maximum Coulomb's force in Fig. 4 is 5ГЧ105 N/m3 at the corner of the HV electrode for ion drag action. When conduction effect is added, the maximum Coulomb's force is weakened because negative charges are collected near the positive HV electrode. Although the maximum Coulomb's force is weakened, the developed pressure in Fig. 6 increases by 36

The maximum electric field strength in Fig. 7 is 15 MV/m on the charge injection region of the positive HV electrode. The electric field strength is not affected by conduction effect although not shown in the figure.

Two-plate electrodes mounted on wall

The distributions of charge density, Coulomb's force and pressure are shown in Figs. 8-10. The cases for only ion drag, only conduction and both actions are compared. The applied voltage is +2.0 kV and the flow rate is zero.

Comparison of Fig. 8(a) to Fig. 8(c-1) shows that the injected charge density distribution changes from a thin, flat shape to a thick, round shape. This change is caused by the conduction flow. In Fig. 8(b), dissociation charges are distributed more widely near the ground electrode than near the HV electrode. This is because the ground electrode is 3.3 times longer than the HV electrode. Such an asymmetric distribution of the charges may generate a net flow for the direction from narrow to wide electrode. This is the well-known working principal of conduction pump, which can be seen from the Coulomb's force distribution in Fig. 9(b). The area where the Coulomb's force acting to the right on and above the ground electrode is larger than that acting to the left on and above the HV electrode. When charge injection is added (Fig. 9(c)), the zero force boundary tilts toward the HV electrode, then Coulomb's force to the ground electrode is enhanced.

As shown in Fig. 10(c), high pressure appears at the left corner of ground electrode when both ion drag and conduction act. The pressure on and downstream the ground electrode for the case of both ion drag and conduction acting is higher than that for the case of only conduction.

Embedded two-plate electrodes

The distributions of charge density, Coulomb's force and pressure are shown in Figs. 11-13, respectively and are very similar to those for the two-plate electrodes mounted on the wall.

As with the mounted plates, dissociation charge occupies whole of the channel (Fig. 11(c-2)), so the Coulomb's force induced by the dissociation charge covers wide range of the channel (Fig. 12). In Fig. 13, high pressure area appears near the HV

electrode in case of only conduction flow, on the other hand, the area is near the ground electrode in case of the both ion drag and conduction flow. This change is because the charge injection from the HV electrode make pressure near the ground electrode high and weaken the Coulomb's force induced by the dissociation charge near the HV electrode.

Comparison of pressure - flow rate characteristics

Fig. 14 presents simulated pressure - flow rate characteristics for the three electrode configurations. The pressure difference between the outlet and inlet of the channel is plotted at different flow rates. The net flow direction is from left to right in Fig. 1. In Fig. 14(a), the pressure developed by the ion drag action is higher than that by conduction action, while the situation is reversed in Fig. 14(b) and (c). In all configurations, the pressure developed by both ion drag and conduction actions is the highest. At zero flow rate in Fig. 14(a), the developed pressure is 29 Pa for only ion drag action, is 5 Pa for only conduction action, and is 40 Pa for both actions. When the ion drag and conduction act simultaneously, the developed pressure is augmented and is higher than the sum of the pressures developed separately by each action. The augmentation effect in Fig. 14(b) is the largest of all. In Fig. 14(b), the developed pressure for ion drag action is 4.9 Pa. On the other hand, the conduction action develops 12 Pa. When the ion drag and conduction act simultaneously, the pressure increases to 49 Pa. This pressure augmentation may result from the variation of the CoulombвЃ™s force distribution in Fig. 9, which is caused by the variation of the dissociation charge distribution induced by the ion drag flow.

5 CONCLUSIONS

This paper investigates numerically the interaction between the ion drag and conduction actions using platevЃ™bar, mounted plates and embedded plates electrodes in two-dimensional channel. It is found that when the ion drag and conduction act simultaneously, the developed pressure is augmented and is higher than the sum of the pressures developed separately by each action. It is also found that the pressure augmentation depends strongly on electrode configuration.

Acknowledgements

The authors would like to express their gratitude to Mr. Yuta OTSUKA for his help in the experiment. This research was partially supported by JSPS KAKENHI Grant number 16K06076.

References

[1] M. Nishikawara, M. Shimada, M. Saigo, and H. Yanada, Numerical investigation into characteristics of an ion drag pump, Journal of Electrostatics, Vol. 84, pp. 23-31, 2016.

[2] M. Yazdani, J. Seyed-Yagoobi, Effect of charge mobility on dielectric liquid flow driven by EHD conduction phenomenon, Journal of Electrostatics. Vol. 72, pp. 285вГ Y294, 2014.

[3] M. Yaszdani, J.Seyed-Yagoobi : The effect of uni/bipolar charge injection on EHD conduction pumping, Journal of Electrostatics, 75,43/48 (2015)

[4] H. Yanada, T. Yamada, Y. Asai, Y. Terashita, Measurement and numerical simulation of ion drag pump characteristics, Journal of Fluid Science and Technology. 5 (2010) 617вГ Y631.

[5] JIS C 2101, Testing Methods of Electrical Insulating Oils, 1999.

[6] J.K. Park, J.C. Ryu, W.K. Kim, K.H. Kang, Effect of Electric Field on Electrical Conductivity of Dielectric Liquids Mixed with Polar Additives: DC Conductivity, The Journal of Physical Chemistry B. 113 (2009) 12271вГ Y12276.

[7] Material Safety Data Sheet of DBS, available at: http://www.daihachi-chem.co.jp/msds/list.html, Daihachi Chemical Industry Co.,Ltd., last (accessed 08.07.16).

Masahito, Nishikawara, D2-202, Building D2, 1-1, Hibarigaoka, Tenpaku-cho, Toyohashi, Aichi, 441-8580, Japan